Characterization Of The Non-Reacting And Reacting Flow On A Low-NO_x GT Combustor With Enhanced Internal Mixing Mechanism

José Manuel das Neves Rodrigues

Instituto Superior Técnico, Technical University of Lisbon, Aerospace Department

The present work reports the numerical analysis of the non-reacting and reacting flow of a Low-NO_x GT combustor with intensive internal mixing mechanisms. From this analysis, the performance of the numerical model in reproducing the reacting flow and the mixing mechanisms is highlighted. The unsteady flow was computed with two URANS turbulence models – the standard $k-\varepsilon$ and a RSTM model – and the PaSR combustion model, implemented in OpenFOAM®, with the skeletal Smooke chemical mechanism. The grid and the effects of the turbulence models on the numerical solution were also investigated and the results compared with experimental data. In addition, the PaSR combustion model was tested and validated with a lifted turbulent diffusion flame test case, well documented in the literature. Three chemical mechanisms were used along the combustion model, namely the 2-step Westbrook and Dryer mechanism, the skeletal Smooke mechanism and the detailed GRI-2.11 mechanism. The results of the non-reacting flow showed good agreement with experimental data. The PaSR combustion model generally over predicted the temperature field, either in the reacting flow inside the combustor or in the lift-off flame test. Despite the poor correlation with the measurements, the reacting-flow predicted inside the combustor yielded the fundamental working characteristics of flameless combustion.

INTRODUCTION

The massive release of greenhouse gases (GHG) to the atmosphere has been pointed out as the well-known reason for the climate change the Earth's ecosystem is facing today. Aircraft traffic contribution to anthropogenic CO_2 emissions was around 2.4% in 2006, in the U.S. alone [1], but, with the increasing demand on air travel, this contribution keeps growing at a fast rate. CO_2 is a natural product of the complete oxidation of any carbon-based fuel and the only way to reduce emissions is by improving the engine's thermodynamic cycle efficiency. Increasing pressure-ratio is a method generally used in gas turbines to improve cycle efficiency. However, this approach yields high combustion air temperature and, therefore, high flame temperatures, promoting formation of nitrous oxides, NO_x – another hazardous pollutant threatening climate and human health. Levy *et al.* [4] proposed a novel combustor concept to achieve ultra-low NO_x emissions, with application to aircraft gas turbines – the FLOXCOM® adiabatic combustor. This combustor takes advantage of a combustion regime called flameless combustion, devised by Wünning and Wünning [5]. The flameless combustion mode is characterized by high recirculation rates of combustion products (higher than 1) and a large and uniform reaction zone. The large concentration of burnt products and low oxygen levels in the reaction zone induce much slower combustion rates and, consequently, smoother temperature and species gradients. On the other hand, the burnt products, due to their high heat capacity and to the heat exchange with the incoming fresh air, maintain the reaction region temperature at a fairly uniform distribution and relatively low (typically bellow 1850 K).

Figure 1 illustrates the working principle of the FLOXCOM® combustor. At junction 2 the fresh combustion air is diluted in the recirculated burnt products. Once the combustion products are well diluted in the new combustion air, fuel is injected and mixed with the reacting mixture at junction 3. An important requirement of this combustion type is to avoid fuel injection before perfect dilution of air and burnt gases. If the vitiated mixture temperature exceeds the fuel auto-ignition temperature, it ignites spontaneously and continuous combustion is sustained. The temperature profile develops uniformly across the reaction zone, with the maximum temperature being typically lower than 1850 K and temperature gradients not higher than

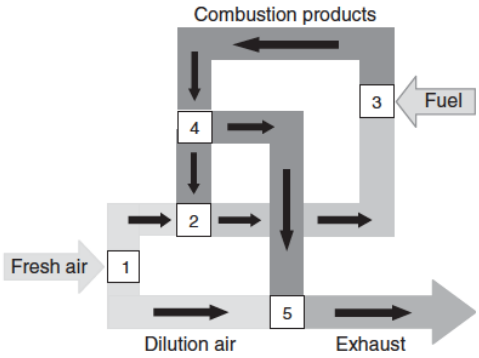

Figure 1 - Working principle of the combustor, Melo *et al.* [4]

200 K. Accordingly, no strong species gradients are detected, and the heat of combustion is evenly released through the reaction region. With this combustion conditions, no luminosity or sound emission is distinguished and, for this reasons, the resulting combustion regime is called flameless oxidation [5]. At junction 4, part the combustion products are recirculated back to the reaction region (junction 2) and the remaining leaves the combustor through the exhaust at junction 5. To cool down the hot exhaust gases, part of the fresh air inlet stream is directed straight to the dilution channel. This is an important requirement for GT combustors since the hot exhaust gases can seriously wear out the first turbine stage blades. An important issue of the present design relates to the fact that the latter splitting mechanism, the mixing mechanisms and products recirculation are controlled exclusively by aerodynamic processes, which are still quite unknown. Melo *et al* [6], [7], studied these processes experimentally in six different combustor prototypes based on the FLOXCOM® concept with methane as fuel. He was able to sustain stable combustion for recirculation rates ranging from 0.4 to 1 and equivalence ratios as low as 0.2 and reported very low NO_x emissions for all configurations, most cases below 10 ppm. However, very high concentration of CO and HC at the outlet revealed low combustion efficiency for some configurations. Nonetheless, combustion efficiencies close to 1 (≈0.99) were also registered in one configuration. The study further reports an uniform temperature profile in the combustion zone, with gradients not higher than 200 K, very low oxygen concentration and temperatures not higher than 1850 K, endorsing the principles of flameless combustion.

Several researchers have studied flameless combustion numerically, mostly on simple set-ups like industrial furnaces. It was found that the EDC combustion model combined with a detailed chemical mechanism offers the best matching results with experimental data and that the *flamelets* model is inappropriate to model the flameless combustion regime. Most researchers found that the *k-ε* model is suitable to resolve the turbulence quantities for flameless combustion in an industrial furnace set-up and low recirculation rates, but fails to reproduce the experimental data in the regions near the burner, where the flow gradients are higher [8]. Moreover, some argue that the solution may be optimized if one modifies the $C_{1\varepsilon}$ *k-ε* model constant to 1.6, instead of the standard value 1.44 [9].

In the present work the most relevant flow features leading to the flameless combustion regime, namely the mixing mechanisms efficiency, are investigated. It comprised the numerical simulation of the non-reacting and reacting flow inside a combustor prototype based on the FLOXCOM® principles and the simulation of a lifted turbulent diffusion flame to test and validate the combustion model used.

NUMERICAL MODELING OF THE REACTING FLOW

The Favre averaged form of the conservation equations of mass, momentum and energy were used to solve the reacting and non-reacting flows. To resolve the unclosed Reynolds stresses and turbulent fluxes on the averaged equations, the standard $k-\varepsilon$ turbulence model [10] and the RSTM turbulence model [11] were employed. Both models imply the solution of a turbulent kinetic energy transport equation and an energy dissipation transport equation. In addition, the RSTM model also requires the solution of a Reynolds Stress transport equation, which adds to the model solution more sensibility capturing the secondary motions of the flow. The standard model constant values of each model were considered.

The radiative heat fluxes were computed with the discrete ordinates method (for the lifted flame simulation) and with the P_1-approximation method (for the reacting flow field inside the FLOXCOM® combustor). The properties of the medium were determined assuming a grey gases mixture and a transparent gas. Only CO_2 and H_2O were considered as absorbent gases and the values of $a_{\varepsilon,i}$ and k_i were extracted from [12] and [13].

Turbulence/Chemistry interaction model

The unclosed species consumption/production term in the averaged species equation, $\overline{\dot{\omega}_k}$, was closed with the Partially Stirred Reactor model (PaSR) devised by Karlsson [14]. The PaSR model is the turbulence/chemistry interaction model implemented in OpenFOAM® [15]. The concept of the PaSR ignores the sub-grid laminar structure of the turbulent flame and, considering that real flames are much thinner than any computational cell in the domain, it assumes that the entire cell is a perfect reactor [16]. The relation between the unclosed consumption/production rate of species *k*, $\overline{\dot{\omega}_k}$, and the laminar correspondent is given by:

$$\overline{\dot{\omega}_k} = \frac{\tau_c}{\tau_c + \tau_{mix}} \dot{\omega}_k = \kappa \dot{\omega}_k \qquad (1)$$

where τ_c is the chemical timescale, τ_{mix} is the turbulent mixing time and $\dot{\omega}_k$ is the laminar consumption/production rate of species *k*. The turbulent mixing time is determined using the turbulent quantities as follows:

$$\tau_{mix} = C_{mix} \sqrt{\frac{\mu_{eff}}{\bar{\rho}\varepsilon}} \qquad (2)$$

The model constant C_{mix} was set to 0.03 [17]. The chemical timescale is taken from the characteristic

time of the chemical reaction system, which consisted of $N \times M$ Ordinary Differential Equations (ODEs). The fuel considered in this study was methane (CH_4) and three chemical mechanisms were employed to describe the chemistry of the methane-air flames: the simplified Westbrook and Dryer two-step mechanism [18], with 2 equations and 5 species; the skeletal methane mechanism of Smooke [19], with 33 equations and 17 species; and the detailed GRI-MECH 2.11 [20], with 277 elementary chemical reactions and 49 species. The GRI-MECH 2.11 mechanism includes nitrogen chemistry relevant to methane chemistry.

NUMERICAL SET-UP

Geometry

The FLOXCOM® is a novel GT annular combustor concept with a very larger recirculation zone, designed to operate in flameless conditions. Even though there are several designs following the basis of the FLOXCOM® combustor, we focused this investigation on the prototype studied by Melo [6], in IST, shown in Figure 2. The prototype consists of a 60-degrees wedge-section of the total annular

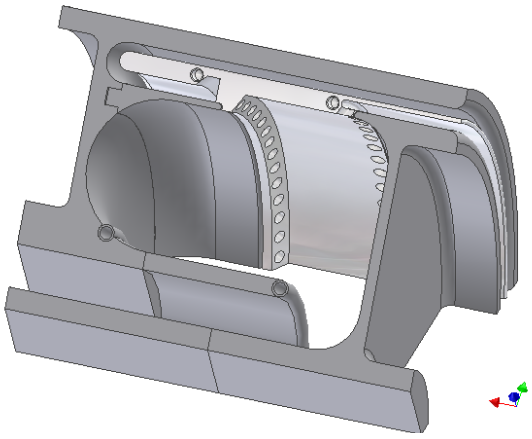

Figure 2 - CAD representation of the FLOXCOM® combustor prototype [6].

combustor. The longitudinal cross-section is sketched in Figure 3. The colored area in Figure 3 highlights the combustion zone, dilution zone and exhaust, which, combined, correspond to the numerical domain considered for the analysis. Pre-heated air enters the combustion chamber through the Right inlet, with 14 injection holes at 210º relatively to the radial direction, and through the Left inlet, with 14 injection holes at 120º relatively to the radial direction. The air injection holes from both sides have 4 mm diameter and are arranged in a staggered arrangement with uniform spacing. The fuel is injected at 45º from the radial direction through 15 injection holes evenly distributed in the tangential direction, with an internal diameter of 2 mm. The dilution zone and the exhaust opening are located in the inner radius of the combustor, as illustrated in Figure 3. Notice that the air mass flux through each air entrance is equal, being exactly half of the total airflow reaching the combustor. This allows us to disregard the flow inside the channels upstream of the combustor from the numerical domain.

Operating Conditions

In [6], several sets of operating conditions were tested. For the interest of this investigation, only the configuration leading to the flameless combustion regime with ultra-low levels of NO_x and higher overall efficiency was selected. Table 1 summarizes the operating conditions chosen for the analysis:

Total airflow	1.7 m^3/s @ atmospheric pressure and pre-heated to 425 K
Fuel	Methane (CH4) @ 293 K
Equivalent ratio	0.28

Table 1 - Operating conditions [6].

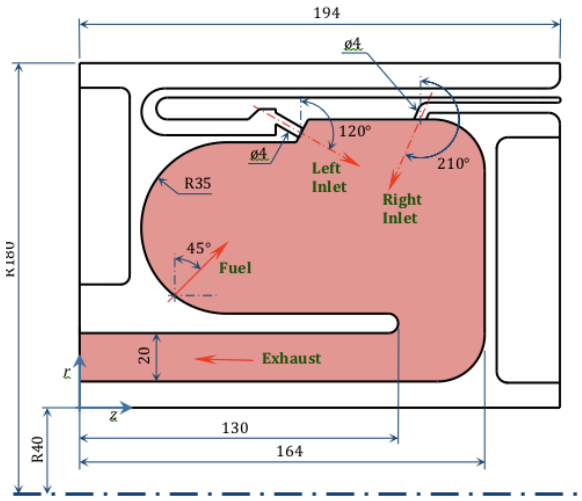

Figure 3 - Cross-section of the FLOXCOM® combustor prototype [6].

Grid

To spare some computational effort, one can take advantage of the axisymmetric domain and reduce the computational domain to a smaller section of the original 60-degrees combustor. For this effect, periodic boundary conditions must be implemented at each bounding faces to virtually represent the flow that is not numerically represented, keeping the integrity of the numerical domain relatively to the original 60-degrees domain. In order to evaluate the validity of this approximation/abbreviation of the domain, three sections with 60/14-degrees (section A), 180/14-degrees (section B) and 30-degrees (section C) were considered, corresponding to $1/14^{th}$, $3/14^{th}$ and 1/2 of the original 60-degrees section.

Accordingly, on the Left and Right inlets, section A has one hole, section B has three holes and section C has seven holes, with the number of fuel injector holes following the same distribution.

Unstructured grids were used for all three sections. Even though there is some loss in accuracy with the unstructured grid, fitting a structured grid in such complex geometry is very cumbersome and time consuming. On the other hand, with the unstructured grid, we easily fit a structured grid layer near the wall and around the recirculation zone, so that the flow stays aligned with the grid and the high gradients near the wall are better resolved. The grids consist of hexahedron elements only. The mesh of section A has 39508 cells, section B has 109384 cells and section C has 253878. Because the elements used are hexahedron, for convenience, the section of both air and fuel inlets was changed to a square, with an equivalent area as the original circular inlet. All the grids were set up with the Gambit® software package and then exported to OpenFOAM®.

Numerical Procedure

An implicit pressure-correction algorithm, the PISO algorithm, was used to solve the unsteady flow field. The flow field equations were discretized with the MUSCL scheme, except for the radiative heat transfer equation that was discretized with a linear upwind differencing scheme. The second-order MUSCL convective scheme is ideal to resolve the strong gradients generated by the highly turbulent flow, not only near the combustor walls, but mainly in the region where the inlet combustion air jets and recirculating products interact. Furthermore, as the flow is mostly aligned with the grid in the recirculation zone, less discretization errors are expected.

For the simulation of the reacting flow simulation in the FLOXCOM® combustor, the domain was discretized with of Section B, the skeletal Smooke mechanism was used to describe the chemistry system and the RSTM turbulence model was considered to resolve the turbulent flow. The numerical procedure carried out to obtain the converged solution of the reacting flow comprised two steps: (I) starting with the non-reacting flow solution as initial solution, the reacting flow computation was undertaken with the standard $k-\varepsilon$ turbulence model until the solution became statistically stable. Then, (II) using the solution obtained previously, the simulation was restarted with the RSTM turbulence model and the P_1-approximation to solve the radiative heat equation.

The convergence criteria were based on the residuals of the equations being solved. For the simulation obtained with the standard $k-\varepsilon$ model, the solution was considered converged when continuity, momentum and turbulent kinetic energy equations residuals were lower than 1×10^{-5}. For the simulations with the RSTM, because of the unsteadiness of the Reynolds-stress transport equation residuals, the convergence criterion was additionally based on the total mass-flux imbalance of the computational domain, such that convergence was attained when the mass-flux imbalance was lower than 10^{-7}, and the former criteria were also matched. All simulations in this work were carried out until the solution field converged to assure the best possible quality of the numerical results.

Initial and boundary conditions

The boundary conditions were determined based on the operating conditions listed on Table 1. The mass flux and inlet temperature are fixed at all inlets. At the outlet, pressure is fixed and set to the ambient pressure. The inlet air was approximated as an ideal mixture composed by 21% of O_2 and 79% N_2 in volume fraction. The initial turbulent fields were estimated considering a turbulent intensity of 10% and a length scale of $1/100^{th}$ of the recirculation region diameter. The initial solution for the simulations with the RSTM turbulence model were taken from the solution field obtained with the standard $k-\varepsilon$ turbulence model. According to [4], the FLOXCOM® concept was devised considering adiabatic walls and, therefore, the heat flux through the walls was neglected and a zero-gradient boundary condition was assigned for temperature at the walls. Moreover, the walls were treated as opaque and diffusive, with emissivity set to 0.7.

RESULTS AND DISCUSSION

Solution dependency on grid and turbulence models

This section highlights the effects of the axisymmetric domain abbreviation with periodic boundary conditions and the effect of both the standard $k-\varepsilon$ model and RSTM turbulence models on the numerical solution.

Figure 4 shows the plotted results of the axial, radial and tangential velocity profiles obtained for sections A, B and C with both turbulence models at the center of the recirculation region (z = 0.09 m and θ = 0º). In general, the results show reasonable agreement with the experimental results either with the standard $k-\varepsilon$ turbulence model or with the RSTM model at the considered location. Also, no significant differences are observed relatively to the solutions attained for the three different sections.

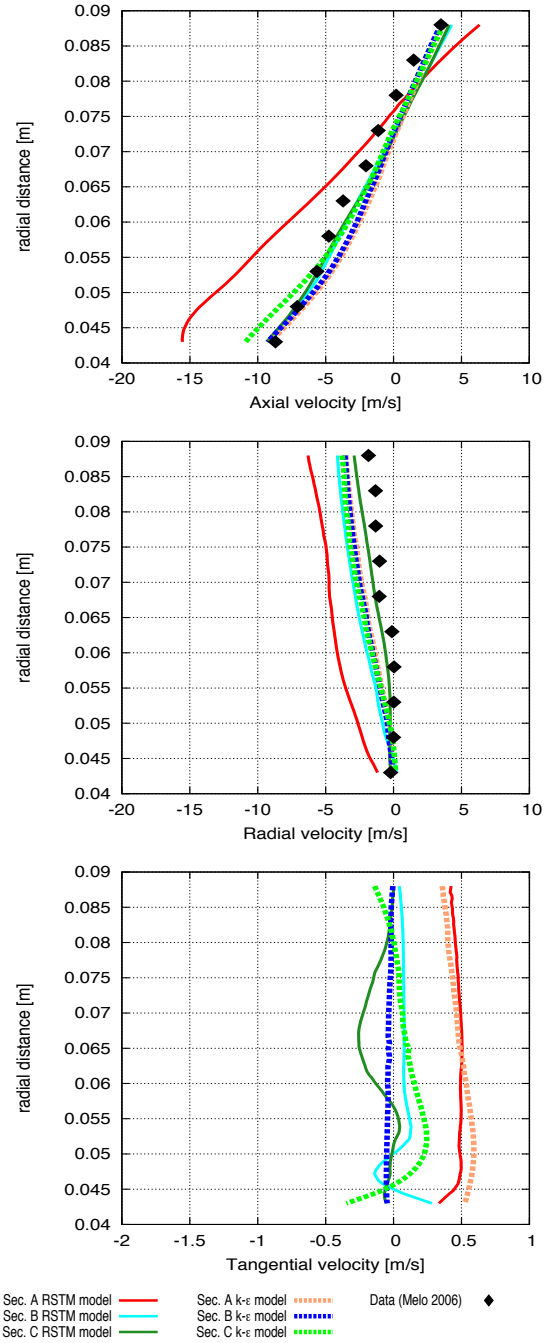

Figure 4 - Axial, radial and tangential velocity fields at the center of the recirculation region of sections A, B and C, obtained with the standard $k-\varepsilon$ and the RSTM turbulence models, with experimental data.

Even though there were no measurements available for the tangential velocity component at any location of the combustor, Melo [6] verified, with LDA measurements in a slightly tilted plan from the mid-plane, that the tangential velocity component is of much lower order of magnitude than the axial and radial components. Thus, the predicted tangential velocity profile in Figure 4 shows consistent with the latter experimental observation, yielding values not higher than 0.5 m/s.

The velocity profiles predicted with the standard $k-\varepsilon$ turbulence model for the three different sections showed only minor differences, implying that the abbreviation of the domain has little influence on the converged numerical solution for this model. On the other hand, with the RSTM model, the solution of the narrower Section A revealed relatively large deviation from the experimental results and the remaining numerical results, whilst the solution of the widest Section C exhibited the best match with the experimental data of all numerical solutions, particularly for the radial velocity component, as verified in Figure 4. It is believed that this is owned to the enhanced sensibility of the RSTM model to the secondary flow motions. Unlike the standard $k-\varepsilon$ turbulence model, the second-order RSTM turbulence model has a transport equation for each Reynolds-stress component and, as a result, the final solution is more sensible to the secondary flow motions developing in the tangential direction.

In general, the solutions obtained for all sections with either turbulence models were fairly similar, showing only minor discrepancies. Thus, the numerical solution is little influenced by the abbreviation of the numerical domain and, accordingly, one can infer that it is possible, to a certain extent, to take advantage of the axisymmetric geometry of the combustor to reduce the size of the computational domain using periodic boundary conditions, without losing the integrity of the numerical solution.

Non-reacting flow field of the FLOXCOM® combustor

The following paragraphs describe the non-reacting flow inside the FLOXCOM® combustor, with emphasis to the velocity fields and turbulence quantities. This investigation is based on the numerical results obtained with section B and the RSTM turbulence with the operating conditions listed in Table 1. The Reynolds number of the flow at the specified operating conditions and based on the recirculation region diameter, D_R = 70 mm, is 22242, evidencing a strong turbulence flow. Figure 5 and Figure 6 show the magnitude contours of the mean velocity field and the corresponding vector orientations at two different meridian planes: the central plane of the combustor (also the symmetry

plane), cutting the Left inlet, and a second plane slightly tilted back around the combustor's revolution axis, cutting the Right inlet.

Figure 5 and Figure 6 highlight two recirculating flows: a primary recirculating flow occupying 60-70% of the combustor's volume (excluding the exhaust channel) and a smaller but stronger recirculating motion occupying about 15-20% of the combustor volume and located just downstream the Right inlet. The larger recirculating motion is the key region of the FLOXCOM® combustor concept and its purpose is to generate a homogeneous hot mixture of fresh combustion air and burnt products and hold stable flameless combustion. The smaller counter-clockwise flow motion is a parasite flow behavior, resulting from the interaction between the Right inlet jets and the stagnant air on the right of the jets. In fact, this unwanted flow effect dissipates a considerable amount of the energy and momentum carried in by the jet and, as a result, the primary recirculating flow becomes weaker.

The clockwise motion of the large recirculation region is controlled mainly by the Right inlet jets, as showed on Figure 5, "pushing" fresh combustion air towards that region. On the other hand, the Left inlet jets drags a portion of the entrained combustion products towards the exhaust channel while it also transfers some of its momentum to the recirculation motion, owed to the viscous effects. Furthermore, the interaction between both the Left and Right inlet

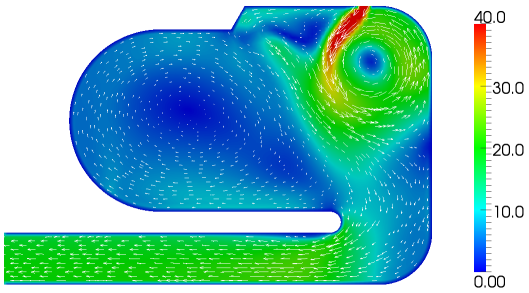

Figure 5 - Contour of the mean velocity field at the meridian-plane cutting the Right inlet. Units m/s.

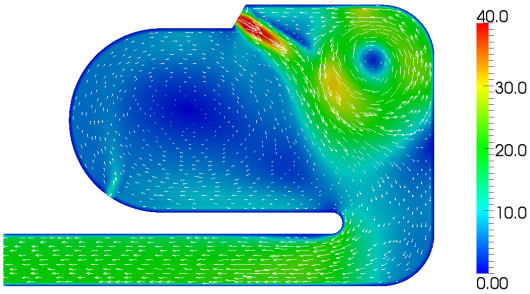

Figure 6 - Contour of the mean velocity field at the mid-meridian-plane, cutting the Left inlet. Units m/s.

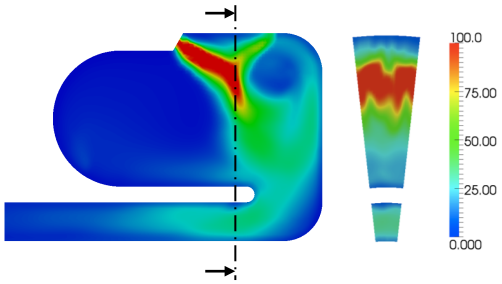

Figure 7 - Turbulent kinetic energy contours at an intermediate meridian plane between both inlets and a transverse plane at $z = 120$ mm. Units m^2/s^2.

jets allows some fresh air to be directed straight to the dilution channel, as one can infer from the vector orientations of Figures 5 and 6. This stream is important to cool down the exhaust gases and homogenize the temperature profile at the outlet.

Figure 7 displays the turbulence kinetic energy contour at an intermediate meridian plane between both inlets and the transverse plane A at $z = 120$ mm. As observed in Figure 7, a strong turbulent stream develops from the high-speed jets through the Left inlets. This turbulent flow is then transported downstream to the dilution zone and some to the recirculation region. The strong fluctuations associated to the turbulent flow promote fast mass diffusion, which benefits the mixture between fresh air, combustion products and fuel and increases the contact area between fuel and oxidant, enhancing combustion efficiency. Thus, it is expected that turbulence at the entrance of the recirculation region and being transported inside the reaction zone will play an important role in the reaction rates and in the overall combustion efficiency. As seen on Figure 7, the Right inlet jets produce little turbulent stresses as they develop towards the interaction zone, comparing with the Left side jets. A possible explanation has to do with the fact the parasite recirculating motion attached to the exit of these jets is dissipating most of the kinetic energy and momentum, attenuating turbulent intensity. Further downstream, due to the dissipative viscous effects, the turbulent fluctuations lose their intensity as they penetrate more into the combustor, as observed in Figure 7.

Even though it was mentioned that the turbulent fluctuations accelerate mass diffusion, improving mixture rates and, thus, reaction rates, they also introduce some advert effects. In fact, the presence of periodic pressure fluctuations induced in the turbulent flow introduces low frequency noise and increased pressure drop during operation. These advert consequences comprise a big impact on the aerodynamic efficiency of the combustion chamber.

Simulation of a lifted non-premixed turbulent flame in OpenFOAM®

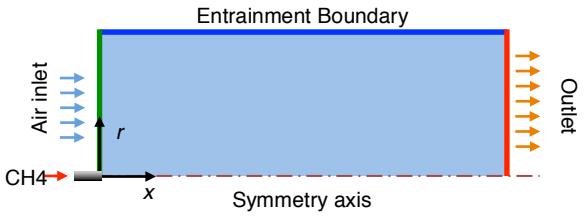

Figure 8 – Numerical domain and boundary conditions enclosing the lifted flame.

A lifted non-premixed turbulent flame was used to validate the reacting flow module on OpenFOAM®. It consist of a free jet methane flame discharging into still air through a burner with a inner diameter, D, of 5 mm. The reference work for this validation is the flame studied experimentally and numerically by Mahmud [21]. The computational domain is an axisymmetric plane with the symmetry axis coincident with the axis of the burner, as in Figure 8. The outlet boundary is located at $200D$ from burner exit and the entrainment boundary, parallel to the symmetry axis, is placed at $50D$ from the axis. The grid had an element density similar to the grids used in [21] and comprises 140 elements in the axial direction and 50 elements in the radial direction. According to [21], this grid configuration is sufficiently fine to reproduce acceptable grid independent solutions. Turbulence was modeled with the standard $k-\varepsilon$ turbulence model with the default constant values. Three chemical mechanisms were tested – the simplified Westbrook and Dryer 2-step mechanism, the skeleton Smooke mechanism and the detailed GRI-2.11 mechanism. The discrete ordinate method was implemented to solve the radiative heat transfer. A uniform axial velocity profile with magnitude equal to 46.4 m/s and zero radial velocity was imposed at the fuel inlet. At the combustion air inlet, inlet velocity was set to 0.8 m/s in the axial direction. The temperature on both inlet boundaries was set to the ambient temperature T_0=293K. The turbulence fields at the boundaries and at the initial time-step were estimated assuming 10% of turbulent intensity and 1/3rd of the burner radius for the turbulent length scale. Every boundary was considered as a black surface at ambient temperature.

Figure 9 shows the temperature contours of the lift-off flame computed with the Westbrook and Dryer 2-step mechanism, the Smooke mechanism and the GRI-2.11 mechanism, Figure 10 exhibits experimental data [21] and predictions of the axial profile of temperature, oxygen and methane along the symmetry axis. Overall, the estimated temperature and oxygen distribution obtained with the Westbrook and Dryer 2-step mechanism and the Smooke mechanism were fairly similar over the entire numerical domain, with only residual differences, whereas the solution with the GRI-2.11 mechanism, although also similar to the solution of the other chemical mechanisms near the burner, exhibited a slight temperature decay in the trailing region of the flame, as observed in the temperature contours and the profiles presented. The lift-off heights resolved numerically, listed on Table 2, show reasonable agreement with the experimental results, indicating that the PaSR combustion model reproduces the detached flame appropriately, regardless the chemical mechanism used. Moreover, the temperature contours on Figure 10 show that a non-reacting region near the symmetry axis penetrates into the flame and pushes the flame front near the axis further downstream. As evidenced in the axial profiles along the symmetry axis of Figure 10, the maximum penetration distance measured in the numerical solutions is roughly between 0.24 and 0.28 m from the burner, depending slightly on the chemical scheme used.

	Westbrook and Dryer	Smooke	GRI-2.11	Data (Mahmud 2007)
Lift-off height, h_{LO}	0.137	0.128	0.139	0.127

Table 2 - Lift-off heights measured from the numerical results and determined from the experimental data

The predicted temperature profiles are appreciably higher than the experimental data. The predicted profiles taken along the symmetry axis of the flame show a sharp temperature rise at the flame front, while the experimental data yielded a rather smoother temperature rise. Likewise, the oxygen and methane concentration levels at the flame front quickly drop and maintain at virtually null levels inside the flame, despite the measured oxygen levels show a much smother evolution and are not lower

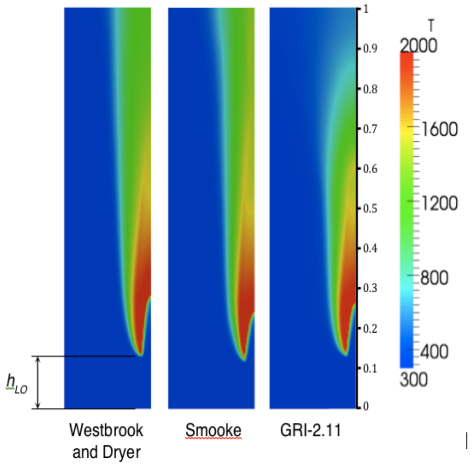

Figure 9 - Temperature contour of the lift-off flame computed with the PaSR model and the Westbrook and Dryer 2-step mechanism, the Smooke mechanism and the GRI-2.11

than 5% at the same locations.

The reported results obtained with the PaSR model reveal, in general, relevant inconsistencies with the measured data. On one hand, the sharp depletion of oxygen and methane at combustion onset suggests that the PaSR combustion model severely amplifies the reaction rates in the fuel-rich regions near the burner, resulting that all oxygen and methane available are immediately consumed at the flame front. On the other hand, the reason for the lack of oxygen inside the flame denotes that the numerical model is not be able to capture appropriately the air (and oxygen) entrainment into the flame near the burner, preventing fresh air from reaching the flame core. Likewise, this may also explain the high flame temperatures predicted in the numerical solution, provided that the dilution of the surrounding fresh air with the reacting flow reduces flame temperatures. The deficiencies identified previously may be attributed to a combination of the limitations in the combustion model and the turbulence model. It is well known that turbulence and combustion are two strongly coupled phenomena and should be analyzed together. As concluded by Peng [17] in his work with diesel spray turbulent combustion, one of the reasons for the discrepancies between the numerical and experimental results obtained with the PaSR combustion model is that the effects of air entrainment and air-fuel mixing might not be well formulated, requiring more improvement,

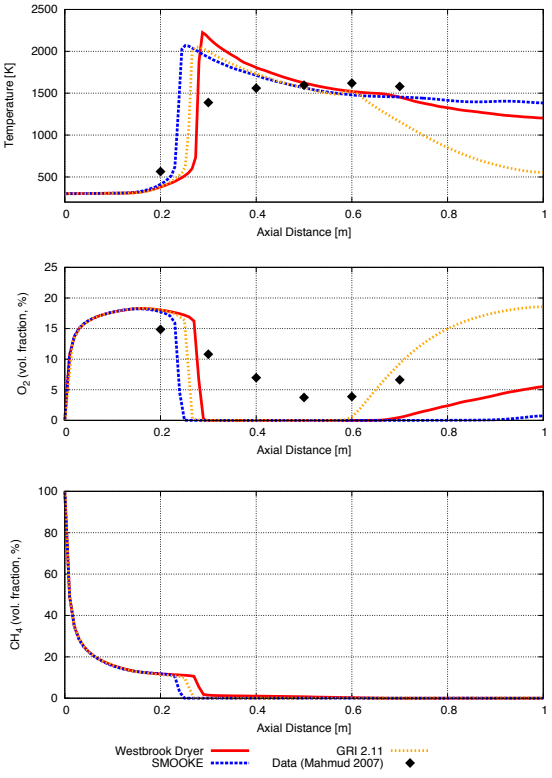

Figure 10 - Predicted and measured axial profiles of the mean gas temperature along the length of the flame.

specifically in the determination of the turbulent mixing time, τ_{mix}, given by equation (1). Several studies concluded that the $k-\varepsilon$ turbulence model under-predicts the turbulence quantities in the regions of high gradients [8] and is responsible for the incorrect prediction of air entrainment into the reacting flow and the air-fuel mixture process in regions near the burner. Thus, flame strain is considerable under-predicted, leading to a much thinner flame front with sharper temperature and species profiles, as pictured in the present numerical results, rather than much smoother profiles and larger flame fronts, typical of turbulent combustion with high flame strain rates.

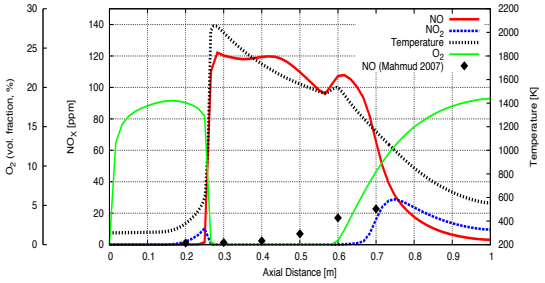

Figure 11 – NO, NO_2, O_2 and temperature predictions and NO experimental measurements along the central axis, obtained using the GRI-2.11 chemical mechanism.

As evidenced in Figure 11, the temperatures considerably high above 1850 K, estimated with the GRI-2.11 chemical mechanism with nitrogen chemistry included, triggered the intense formation of thermal-NO at the flame front. At the location x = 0.7, as oxygen becomes available, the transported NO is re-oxidized, producing NO_2, as illustrated by the dashed-blue line in the plot of Figure 11. Because both oxidations of the atmospheric nitrogen are highly endothermic reactions, it is reasonable to admit that the flame temperature decay is owned to energy (heat) consumption of the chemical oxidation reactions producing NO and NO_2. Moreover, it is believed that the small rise in the NO_2 levels at the symmetry axis before the flame front ($0.2 < x < 0.25$) is due to the re-oxidation of NO that is dragged from flame front regions upstream away from the symmetry axis, and reacts with the oxygen present in the non-reacting flow near the symmetry axis, as evidenced by the slight decay at x = 0.15 of the oxygen levels plotted in Figure 11.

Reacting flow field of the FLOXCOM® Combustor

Figure 12 to 14 show the contours of the predicted temperature field, concentration levels of some relevant species and velocity distribution at the central meridian plane. In Figure 12 and 13, the temperature and species contours inside the FLOXCOM® combustor clearly evidence the presence of a large, high temperature region with

uniform temperature and species distribution, corresponding to the reaction region of the combustor. From Figure 14 is also evident the strong recirculation motion of the reaction region. Furthermore, Figure 13 indicates that the reaction zone is scarce in oxygen but rich in combustion products. These features are consistent with the working principles of the FLOXCOM® combustor, as stated by [4], which result in a flameless combustion mode and ultra-low NO_x emissions.

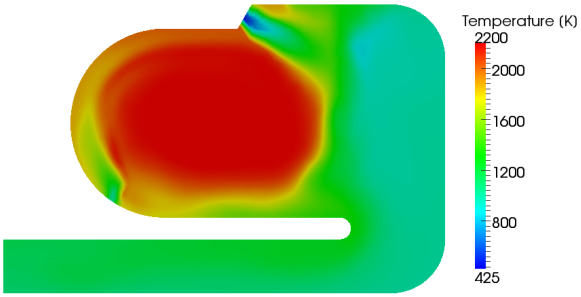

Figure 12 - Predicted temperature contour at the central meridian plane.

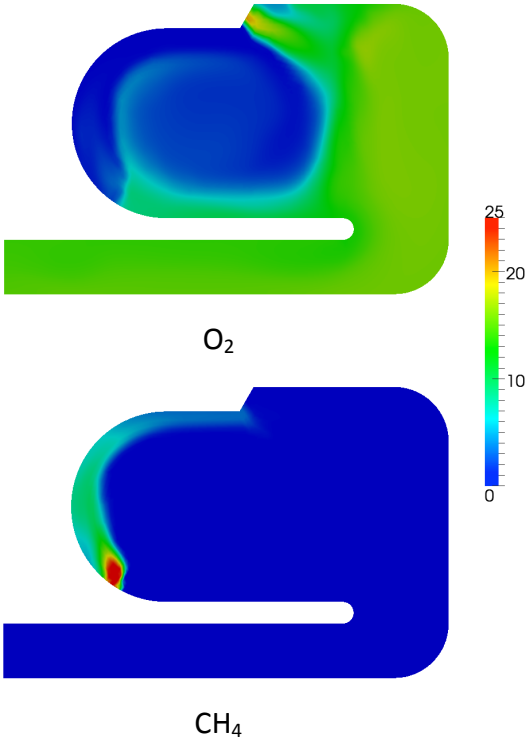

Figure 13 - Predicted concentration levels of O_2 and CH_4 at the central meridian plane [% vol. fraction].

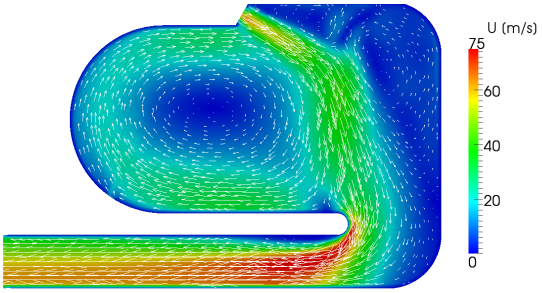

Figure 14 - Predicted velocity contour and vector orientation at the central meridian plane.

As shown in Figure 13, the recirculating motion entrains the fresh combustion air at the combustor entrance and drags it around the reaction region, next to the combustor walls. Simultaneously, the entrained fresh air is diluted in the burnt gases carried by the recirculating flow, increasing its temperature. From Figure 13 it is observed that the fuel is injected in the flow before the oxygen is evenly diluted in the burnt combustion products, violating one principle of the FLOXCOM® combustor concept. Just downstream the fuel inlet, one can identify a region where high methane levels (above 25% in volume fraction) expand over a significant wide area, considering the very small diameter of the fuel injector, suggesting substantial diffusion rates of the methane in the recirculating flow. Furthermore, as the recirculating flow comes across this region, it entrains and dilutes a relevant amount of methane (about 10% in volume fraction). It is believed that the strong fuel jets injecting normally to the main recirculating flow greatly enhances mass diffusion and the mixing rates between oxygen and fuel. Therefore, with the cross-flowing jets configuration, air-fuel mixing mechanisms are much efficient and, consequently, due to the strong and fast recirculating flow and to the more efficient mixing mechanism, the combustion reactions are spread over a wider region.

Figure 15 shows the radial profile at the center of the reacting region (z = 0.09 m, θ = 0º and 0.043 < r < 0.103 m) of the concentration levels of some relevant species. The oxygen levels profile in the core of the reaction zone is, in fact, roughly constant for 0.058 < r < 0.093 m and not lower than 2% in volume fraction. Moreover, the levels of the remaining species are also roughly uniform at the same location, emphasizing the homogeneity of the reaction zone. Even though a large reaction zone might evidence excessive flame strain rates, which typically lead to unstable combustion and eventually blow-off, the recirculating region is able to hold combustion mostly because the temperature of the

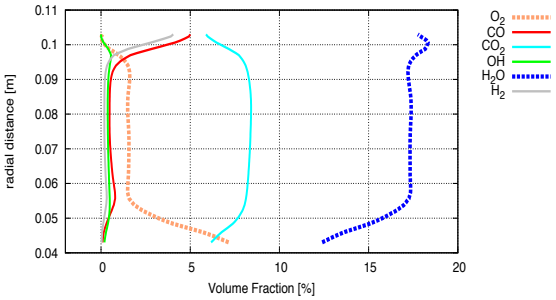

Figure 15 - Radial profile at the center of the reacting region (z = 0.09 m, θ = 0º and 0.043 < r < 0.103 m) of the concentration levels of some relevant species.

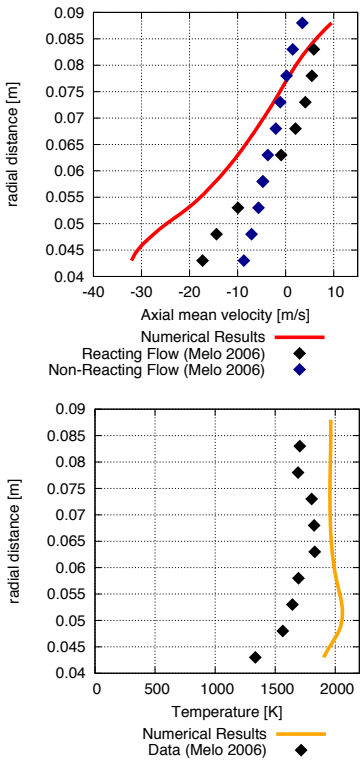

Figure 16 - Data and predicted results of the axial velocity and temperature profiles at the center of the recirculation region ($z = 0.09$ and $\theta = 0$)

vitiated flammable mixture is above the auto-ignition temperature of the fuel.

Despite the numerical solution presents most of the features required for flameless combustion and suitably reproduced the mixing mechanism, the estimated temperature distribution in the reaction region is much higher than the experimental data. In fact, Figure 12 and Figure 16 reveal an average temperature around 2200 K, whereas the maximum temperature registered in [6] was about 1850 K (Figure 16), which is the known temperature limit from which is triggered intensive thermal-NO formation. As outlined before, this might be owned to the fact that heat loss through the walls is disregarded and to the incorrect prediction of the reaction rates as a result of the inadequate treatment of the turbulence/chemistry interaction formulated in the combustion model.

The numerical results indicate that the strength of the main recirculating flow is significantly higher in the reacting flow. As Figure 16 evidences, this behavior is consistent with the experimental observations, although the numerical solution considerably over-predicts the momentum of the recirculation flow. It is believed that the latter over-prediction is related to higher extra thermal expansion of the fluid induced by the over estimated temperature field.

The velocity vector orientation in Figure 14 indicate that a large amount of inlet air is directed straight to the dilution exhaust. This is an important flow feature for a GT combustor since the fresh air flowing directly towards the dilution zone decreases the temperature of the exhaust combustion products and homogenizes the temperature profile at the outlet, protecting the first stage turbine blades from excessive thermal wear.

CONCLUSIONS

The numerical model was not sufficient to solve the temperature profiles and the air-fuel mechanisms in the reacting flow, mostly due to the inappropriate formulation of the combustion model. On the other hand, the non-reacting flow was well predicted by the numerical model with the $k - \varepsilon$ model and the RSTM turbulence models. The effect of the turbulence models and the three meshes in the numerical solution was fairly residual. In the non-reacting flow of the FLOXCOM® combustor, one can identify two recirculating motions: the main recirculation flow occupying most of the combustor's volume and a secondary recirculating flow attached to the Right inlet. The Right inlet jet is responsible to "push" fresh combustion air towards the recirculating region, while the Left inlet jets entrains a portion of the combustion products towards the exhaust channel and transfers some of its momentum to the recirculation motion, due to the viscous effects. In the lift-off turbulent flame simulation, the numerical solution over-estimates, in general, the reaction rates, leading to unrealistic temperature profiles. It is believed that this as to do with an inappropriate formulation of the turbulence mixing time, and to the incorrect prediction of air entrainment into the interior of the flame. Regardless the shortcomings of the turbulence/chemistry interaction model, the lift-off heights computed with either chemical mechanism showed reasonable agreement with the experimentally measured value. The numerical solution of the reacting flow inside de FLOXCOM® combustor, with the RSTM turbulence model, reproduced appropriately the species entrainment to and within the reaction zone and captured the enhanced mixing mechanisms. Most of the features of the FLOXCOM® combustor concept for flameless combustion, devised by Levy (2004), were identified in the reacting flow. The temperature distribution and species concentration levels inside the reaction region were reasonably uniform, with high amounts of combustion products and low oxygen levels. However, the temperature field determined for the reacting flow inside the combustor was considerable over-estimated, as was the velocity field in the combustion zone due to the greater thermal expansion induced by the greater temperature field.

REFERENCES

[1] U.S. Department of Transportation. (2010). *Transportation GHG Emissions and Trends*. Retrieved from http://climate.dot.gov/ghg-inventories-forcasts/national/us-inventory-structure.html

[2] Lefebvre, A. H., & Ballal, D. R. (2010). *Gas Turbine Combustion* (3rd Edition ed.). New York: CRC Press.

[3] Zeldovich, Y. B., Sandovnikov, P. Y., & Frank-Kamenetski, D. A. (1947). *Academy if Sciences of USSR* .

[4] Levy, Y., Sherbaum, V., & Arfi, P. (2004). Basic thermodynamics of FLOXCOM, the low-NOx gas turbines adiabatic combustor. *Applied Thermal Engineering , 24*, 1593-1605.

[5] Wünning, J. A., & Wünning, J. G. (1997). Flameless Oxidation to Reduce Thermal NO-Formation. (E. Science, Ed.) *Prog. Energy Combustion, Sci , 23*, 81-94.

[6] Melo, M. J. (2006). *Desenvolvimento e Optimização de uma Câmara de Combustão para Turbinas a Gás.* PhD thesis, Instituto Superior Técnico, Departamento de Engenharia Mecãnica.

[7] Melo, M. J., Sousa, J. M., Costa, M., & Y., L. (2009). Experimental Investigation of a Novel Combustor for Gas Turbines. *Journal of Propulsion and Power , 25* (3), 609-617.

[8] Rodi, W. (1984). *Turbulence Models and their applications to hydraulics.* Amsterdam: International Association for Hydraulic Research.

[9] Christo, F. C., & Dally, B. B. (2005). Modeling turbulent reacting jets issuing into a hot and diluted coflow. *Combustion and Flame , 142*, 117-129.

[10] Jones, W. P., & Launder, B. E. (1972). The prediction of laminarization with a two-equation model of turbulence. *International Journal of Heat and Mass Transfer , 55*, 310-314.

[11] Launder, B. E., Reece, G. J., & Rodi, W. (1975). Progress in the Development of a Reynolds-Stress Turbulence Closure. *Journal of Fluid Mechanics , 63* (3), 537-566.

[12] Coppalle, A., & Vervisch, P. (1983). The total emissivities of high-temperature flames. *Combustion and Flame , 49*, 101-108.

[13] Smith, T. F., Shem, Z. F., & Friedman, J. N. (1982). Evaluation of coefficients for the weighted sum of gray gases model. *Journal of Heat Transfer , 104*, 602-608.

[14] Karlsson, J. A. (1995). *Modelling Auto-Ignition, Flame Propagation and COmbustion in Non-stationary Turbulent Sprays.* PhD thesis, Chalmers University of Technology, Göteborg.

[15] OpenCFD. (2011). *OpenFOAM*. Retrieved from http://www.openfoam.com/

[16] Nordin, P. A. (2001). *Complex Chemistry Modeling of Diesel Spray Combustion.* PhD thesis, Chalmers University of Technology, Dept. of Thermo and Fluid Dynamics, Göteborg.

[17] Peng, F. K. (2008). *Numerical Modeling of Diesel Spray Injection, Turbulence Interaction and Combustion.* PhD thesis, Chalmers University of Technology, Dept. of Applied Mechanics, Göteborg.

[18] Westbrook, C. K., & Dryer, F. L. (1981). Simplified Reaction Mechanism for the Oxidation of Hydrocarbon Fuels in Flames. *Combustion Science and Technology , 27*, 31-43.

[19] Smooke, M. D. (1991). Reduced Kinetics Mechanism and Asymptotic Approximation for Methane-Air Flames. *Lecture Notes in Physics. 384.* Berlin: Springer-Verlag.

[20] Smith, G. P., M., G. D., Frenklach, M., Moriarty, N. W., Eiteneer, B., Goldenberg, M., et al. Retrieved from http://www.me.berkeley.edu/gri_mech/

[21] Mahmud, T., Sangha, S. K., Costa, M., & Santos, A. (2006). Experimental and computational study of a lifted, non-premixed turbulent free jet flame. *FUEL , 86*, 793-806.